Acoustic solitons: A robust tool to investigate the generation and detection of ultrafast acoustic waves

Emmanuel Péronne, Nicolas Chuecos, L. Thevenard, Bernard Perrin

PHYSICAL REVIEW B **95**, 064306 (2017)

Acoustic solitons: A robust tool to investigate the generation and detection of ultrafast acoustic waves

Emmanuel Péronne,* Nicolas Chuecos, Laura Thevenard, and Bernard Perrin
Sorbonne Universités, UPMC Univ Paris 06, CNRS, Institut des NanoSciences de Paris (INSP), 75252 Paris cedex 05, France
(Received 4 November 2016; revised manuscript received 3 January 2017; published 14 February 2017)

Solitons are self-preserving traveling waves of great interest in nonlinear physics but hard to observe experimentally. In this report an experimental setup is designed to observe and characterize acoustic solitons in a GaAs(001) substrate. It is based on careful temperature control of the sample and an interferometric detection scheme. Ultrashort acoustic solitons, such as the one predicted by the Korteweg–de Vries equation, are observed and fully characterized. Their particlelike nature is clearly evidenced and their unique properties are thoroughly checked. The spatial averaging of the soliton wave front is shown to account for the differences between the theoretical and experimental soliton profile. It appears that ultrafast acoustic experiments provide a precise measurement of the soliton velocity. It allows for absolute calibration of the setup as well as the response function analysis of the detection layer. Moreover, the temporal distribution of the solitons is also analyzed with the help of the inverse scattering method. It shows how the initial acoustic pulse profile which gives birth to solitons after nonlinear propagation can be retrieved. Such investigations provide a new tool to probe transient properties of highly excited matter through the study of the emitted acoustic pulse after laser excitation.

DOI: 10.1103/PhysRevB.95.064306

I. INTRODUCTION

Solitons are very interesting kinds of waves with particle-like properties. They are solutions of nonlinear propagation equations such as the nonlinear Schrödinger equation or the Kadomtsev-Petviashvili equation. The former one applies to water waves and may explain the occurrences of some unusually high coastal waves. Indeed, when two solitons interact, the wave amplitude may be four times bigger during the interaction than the initial amplitude of the solitons before interaction [1].

It has been demonstrated for several crystals that ultrashort acoustic pulses (UAPs) give birth to solitonlike waves due to the balancing of acoustic dispersion and acoustic nonlinearity after strong optical excitation [2–7]. The propagation of high amplitude UAPs may be described by the Korteweg–de Vries (KdV) equation which is well known to possess very specific solutions, the solitons [8]. However, many physical mechanisms usually encountered during experiments may prevent the formation of *classical* solitons. The term classical is used to distinguish them from dissipative solitons or breathers. It refers to the historical soliton as predicted by the Korteweg–de Vries equation. Solitons are often confused with traveling waves because of similar shapes.

Solitons shorter than 200 fs with strain amplitude above 10^{-3} have been inferred from experimental observations in MgO [3] and Al_2O_3 [6] and could be useful to achieve carrier manipulation [9–11] or magnetic switching [12–14]. However, the absorbed optical power can raise the temperature of the sample so much that the attenuation is not negligible anymore. Moreover, the UAPs are also affected by diffraction [15,16]. However, previous experiments [2–5,7] mainly relied on the observation of discrete features propagating faster than the sound and whose velocities and numbers grow with initial UAP amplitude to sustain the existence of KdV solitons. However, when attenuation [17] and diffraction [18] occur, solitonlike UAPs show similar features without being KdV solitons.

Classical KdV solitons possess very intriguing properties, the most noticeable ones being the following: (1) the KdV soliton strain amplitude η_k has a specific profile given by $\eta_k(z,\tau) = ak^2\cosh^{-2}\{k[z-(c+bk^2)\tau]\}$ (z is the position along the propagation direction and τ is the propagation time), (2) a single parameter k determines the width as well as the amplitude and the velocity of the soliton (a, b, and c are provided later in Sec. IV), and (3) one can show by the inverse scattering method that k^2 is determined by the initial UAP the way bound states are determined by the quantum well profile in a Schrödinger equation. The last property has a very interesting corollary: the UAP shape prior to nonlinear propagation can be retrieved once the arrival time distribution of solitons (i.e., the distribution of k parameters) is measured. Hence, measuring the soliton distribution can provide information on the transient mechanisms of transduction. Moreover, once the soliton profile is known, the linear detection function of the apparatus can be retrieved by measuring the soliton profile.

In this paper, evidence of KdV solitons in ultrafast acoustic experiments is provided by checking the properties mentioned above. The experimental setup, which allows a direct measurement of the surface displacement at low sample temperature without laser jitter limitation, is detailed. The (3 + 1)-dimensional KdV-Burgers equation is introduced to discuss the validity of KdV approximations in the framework of ultrafast acoustics. Acoustic solitons are then evidenced in a GaAs(001) substrate thanks to an accurate comparison between the measured soliton and the theoretical one. Before concluding, the relationship between the initial strain pulse profile and the soliton k distribution is explained and illustrated experimentally.

II. NONLINEAR ULTRAFAST ACOUSTIC SETUP AND SAMPLES

In order to observe ultrashort KdV solitons, we have studied with a pump-probe technique samples composed of

*emmanuel.peronne@insp.jussieu.fr

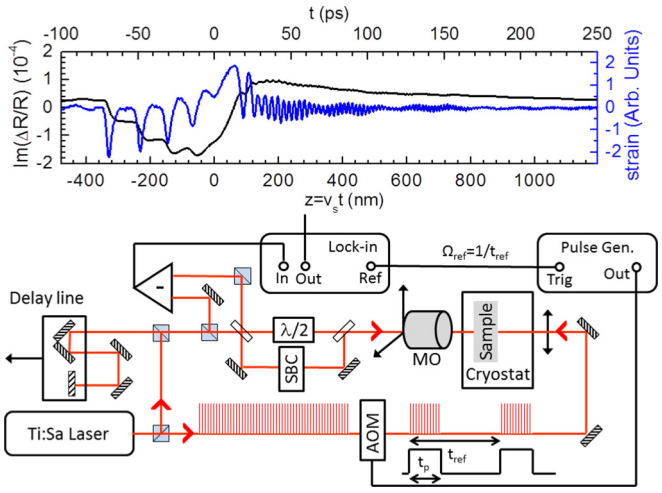

FIG. 1. Pump-probe setup based on interferometric detection of acoustic pulses. AOM: acousto-optical modulator; SBC: Soleil-Babinet compensator; MO: microscope objective; $\lambda/2$: half wave plate. The sample is placed in a cold finger cryostat. Typical pump-probe signal (black line) obtained after photothermal generation in a 60 nm Ti film with 12.5 nJ/pulse, propagation through a 370-μm-thick GaAs(100) slab at 20 K, and detection in a 60-nm-thick Ti layer. The signal derivative (blue line) shows the train of solitons and the dispersive tail.

370-μm-thick GaAs(001) substrates with a thin metallic coating on both sides and placed inside a cold finger cryostat as shown in Fig. 1. The output of a Ti:sapphire oscillator (repetition rate 80 MHz, $\lambda = 750$ nm) is split between pump and probe beams. The pump beam is modulated by an acousto-optical modulator (AOM) which is driven by square pulses with variable duration (t_p) and focused down to $r_s = w_{1/e} = 8$ μm. The probe beam is delayed by t through a multipass linear translation stage and is sent through a Sagnac-type interferometer to measure the complex change of reflectivity of the sample $\frac{\Delta R}{R}$. The probe beam is focused down to 1.6 μm by a microscope objective. The combination of a half wave plate ($\lambda/2$) with a Soleil-Babinet compensator inserted inside the Sagnac loop allows one to set the phase difference to $\frac{\pi}{2}$ where $\frac{\Delta R}{R} \approx i\frac{4\pi}{\lambda_{\text{probe}}}u(r,t)$, $u(r,t)$ being the surface displacement (the photoelastic contribution appears to be negligible for Ti and Cr thin films at $\lambda = 750$ nm). The signal is obtained with a lock-in-phase detection scheme where the modulation frequency Ω_{ref} is used to trigger the pulse generator every $t_{\text{ref}} = \Omega_{\text{ref}}^{-1}$. A typical signal for a 60-nm-thick titanium coating is shown in Fig. 1 (black line) when excited by 12.5 nJ/pulse and cooled down to 20 K. The derivative of the signal shows solitonlike features in the front as expected from previous experiments [2–6] but the dispersive tail is also clearly detected and lasts more than 150 ps. The derivative of the signal is closely related to the strain profile η as discussed in Sec. VI. One can regard the measured strain profile as the in-depth strain profile at fixed delay time (the time to cross the sample) or the temporal strain profile at fixed distance (the thickness of the sample). Position and time are related through the speed of sound v_s such that $z = v_s t$. This is why both scales are used in all the figures of this report.

III. THEORY OF NONLINEAR PROPAGATION OF ULTRASHORT ACOUSTIC PULSES

The propagation of UAPs is advantageously described by a nonlinear equation [2] in paraxial approximation [4]. To extend the validity of this equation it is useful to add phenomenological viscosity [6] $\mu(T)$ (a standard approach in continuum mechanics). Let us note the amplitude η_0, the width z_0, and the lateral extension r_0 of the UAP. The evolution in time τ of the pulse profile along the propagation direction z in a given crystal is governed by a nonlinear equation which is detailed in a previous work (see Ref. [19]). To summarize, it can be expressed in the reference frame moving with the speed of sound v_s as

$$\frac{\partial \eta}{\partial \tau} = -\frac{C_3\eta_0}{2v_s\rho z_0}\eta\frac{\partial \eta}{\partial z} + \frac{F}{2v_s\rho z_0^3}\frac{\partial^3\eta}{\partial z^3} + \frac{\mu(T)}{2\rho z_0^2}\frac{\partial^2\eta}{\partial z^2} - \frac{\xi^2 v_s z_0}{2r_0^2}\frac{1}{r}\frac{\partial}{\partial r}r\frac{\partial}{\partial r}\int_{-\infty}^{z}\eta\, dz', \quad (1)$$

where ρ is the density, C_3 is the nonlinear elastic coefficient (see Ref. [2]), and F is the dispersion coefficient (see Ref. [20]). $\mu(T)$ is the viscosity which may include an effective Herring process coefficient [21] but does not encompass others attenuation processes for UAP in crystals [17,22]. ξ^2 is a (dimensionless) diffraction strength coefficient such that $\xi^2 \neq 1$ when the elastic tensor is not isotropic [4,23]. Equation (1) describes the effect of viscosity and dispersion on the nonlinear propagation of an acoustic pulse with a finite transverse profile within the paraxial approximation. Note that, for a given crystal symmetry, C_3, $\mu(T)$, F, and ξ^2 depend on the direction of propagation and the polarization of the pulse. It can be referred to the $(3+1)$-dimensional KdV-Burgers equation in cylindrical coordinates [19]. Indeed, when the diffraction term is omitted, Eq. (1) is identical to the Burgers equation for negligible dispersion and identical to the KdV equation for negligible attenuation. While the numerical solution of Eq. (1) shows some kind of solitary waves solution, the KdV equation is known to possess specific solitary waves named solitons.

IV. VALIDITY OF KORTEWEG–DE VRIES IN ULTRAFAST ACOUSTIC EXPERIMENTS

Following Ref. [19], it is possible to weight the contribution of each term of Eq. (1) for a given substrate once the initial UAP parameters $\{\eta_0, z_0, r_0\}$ are provided. η_0 is simply the strain pulse amplitude and varies from 10^{-6} to few 10^{-3} in typical ultrafast acoustic experiments. The lateral extension of the initial UAP is usually given by the Gaussian profile e^{-r^2/r_p^2} of the pump spot such that $r_0 = r_p = 8$ μm in this paper.

It may be convenient to define z_0 as $z_0^{-1} = \frac{1}{\eta_0}\max\{|\frac{\partial \eta}{\partial z}|\}$ (see Ref. [19]). A quick survey of several experiments performed in different metallic film transducers provides different values for such definition of z_0: 14.2–22.8 nm in aluminum [3,4] and 14–19 nm in chromium [6] (the differences observed for the same metal are related to the deposition method and to different oxyde layer thicknesses). In order to estimate z_0 for the Ti layer of the sample, experiments at very low pump fluences have been performed when the signal is linear, i.e., scales with the pump power (triangles in Fig. 2). Since Eq. (1) can be solved

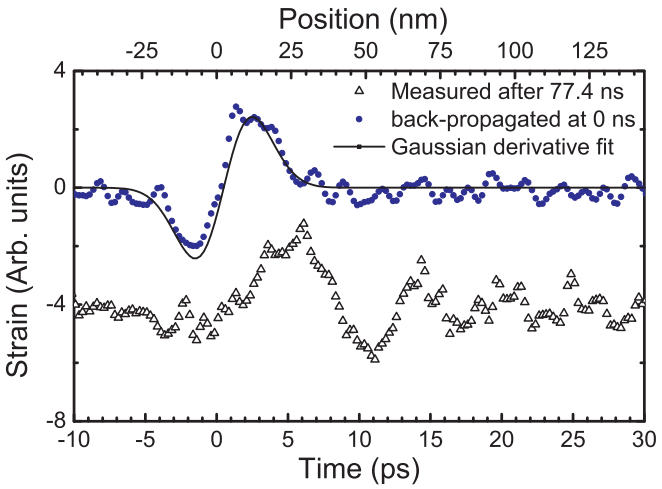

FIG. 2. Strain profile (black triangle) measured at $\tau = \tau_{\text{prop}} =$ 77.4 ns after linear propagation through GaAs(100) substrate at 20 K (DC = 50% with 12.6 pJ/pulse). Initial strain pulse (blue dot) calculated by propagating back numerically at $\tau = 0$ ns the strain profile. The initial strain pulse is well fitted (see text) by a Gaussian derivative (solid line) with $z_0 = 13$ nm.

analytically in the linear regime, it is possible to retrieve the initial strain pulse profile. Figure 2 displays the pulse profile recorded at low pump fluence (triangles) and the numerically back-propagated pulse profile (blue dots). The viscosity has been neglected in the initial strain pulse computation, otherwise the pulse is lost under the amplified noise once back-propagated. The initial UAP profile is then fitted with the Gaussian derivative function $\eta(z,r=0,\tau=0) = \eta_i(z) = \eta_0\sqrt{e}\frac{z}{\delta}e^{-(1/2)(z^2/\delta^2)}$ with relatively good accuracy (see the solid line in Fig. 2). The viscosity is taken into account for the curve fitting by applying a spectral filtering $e^{-(1/2)(\mu\tau_{\text{prop}}/2\rho v_s^2)\omega^2}$. The Gaussian derivative fit is obtained with $\delta \approx 9.6$ nm which gives $z_0 = \frac{e\delta}{2} \approx 13$ nm for a Ti film, a value in line with previous observations in different metallic films (e.g., chromium layers [6]). While the Gaussian derivative profile works nicely for thin titanium and chromium films under low power laser excitation it cannot be extended to other metallic films easily. It is a good approximation in our experiment as long as the pump absorption in the GaAs substrate stays negligible. Indeed, different transduction mechanisms occur simultaneously in GaAs (see Ref. [7] for more details).

Once z_0 has been estimated, each term of Eq. (1) can be evaluated. They are weighted by the constants τ_i^{-1}, $i =$ nl,disp,vis,diff, respectively, whose expressions are given in Ref. [19] and recalled in Table I. The parameters for GaAs(001) at 20 K are chosen as follows: $v_s = 4.78$ nm ps^{-1}, $\rho = 5.32 \times 10^3$ kg m^{-3}, $C_3 = -266$ GPa, $\frac{F}{2\rho v_s} = -7.4 \times 10^{-3}$ nm^3 ps^{-1}, $\xi^2_{[100]} = 2.32$, and $\frac{\mu(20\text{ K})}{2\rho} = 2.4 \times 10^{-4}$ nm^2 ps^{-1}. The viscosity parameter has been estimated by measuring the damping of acoustic pulses propagating linearly back and forth through the substrate at 20 K. For $\eta_0 = 10^{-3}$, τ_{nl} appears to be the only time constant much shorter than the travel time τ_{prop}, while attenuation and diffraction effects are characterized by a time constant much larger than the time it takes for the pulse to propagate

TABLE I. Definitions of τ_i, $i =$ nl,disp,vis,diff. The values are calculated in nanoseconds for a GaAs(001) substrate of thickness $d_s = 370$ μm, $\eta_0 = 10^{-3}$, $z_0 = 13$ nm, $w_0 = 8$ μm, $v_s = 4.78$ nm ps^{-1}, $\rho = 5.32 \times 10^3$ kg m^{-3}, $C_3 = -266$ GPa, $\frac{F}{2\rho v_s} = -7.4 \times 10^{-3}$ nm^3 ps^{-1}, $\xi^2_{[100]} = 2.32$, and $\frac{\mu(20\text{ K})}{2\rho} = 2.4 \times 10^{-4}$ nm^2 ps^{-1}.

τ_{prop}	τ_{nl}	τ_{disp}	τ_{vis}	τ_{diff}
$\frac{d_s}{v_s}$	$-\frac{2\rho v_s z_0}{C_3\eta_0}$	$-\frac{2\rho v_s z_0^3}{F}$	$\frac{2\rho z_0^2}{\mu(T)}$	$\frac{2r_0^2}{\xi^2 z_0 v_s}$
77.4	2.5	297	704	888

through the sample. Assuming that the strain profile remains the same as the one measured at low pump fluence, it seems that the attenuation and the diffraction effects can be neglected. However, since the definition of z_0 depends on the pulse profile which changes under nonlinear effects during the propagation, a finer analysis is required for higher fluences (i.e., in the nonlinear regime).

In fact, at short delays ($\tau < \tau_{\text{nl}} \ll \tau_{\text{prop}}$) the propagation is mainly nonlinear, which means that the UAP evolves into a shock wave which implies a local stiffening of the UAP profile and therefore a decrease of z_0 ($\propto \max\{|\frac{\partial\eta}{\partial z}|\}^{-1}$). By equating τ_{nl} and τ_{disp} one can find that as z_0 approaches $\sqrt{\frac{F}{C_3\eta_0}} \approx 1.2$ nm the dispersion effect becomes significant as well. It prevents the formation of a shock wave by developing acoustic solitons and/or a dispersive tail. In the meantime the viscosity contribution increases as well but not as much as the dispersion ($\frac{\tau_{\text{vis}}}{\tau_{\text{disp}}} \propto \frac{1}{z_0}$). By equating τ_{disp} and τ_{vis} one can find that as long as $z_0 < \frac{F}{\mu(T)v_s}$ (≈ 31 nm), the dispersion effect is always larger. Moreover, when z_0 decreases, the diffraction effect decreases as well so that it can be neglected during the soliton formation. (It is interesting to note the analogy between the Rayleigh criteria and the τ_{diff} criteria.) Therefore, the KdV equation is a good approximation in GaAs at low temperature when using a thin metallic transducer ($z_0 < 31$ nm) and as long as $\tau < \tau_{\text{vis}}$ (i.e., the sample thickness must be such that $\tau_{\text{prop}} < \tau_{\text{vis}}$). One can then expect to observe KdV solitons as mentioned in the Introduction with $a = -12\frac{\tau_{nl}}{\tau_{\text{disp}}}$, $b = \frac{4}{\tau_{\text{disp}}}$, and $c = v_s$. At larger times $\tau > \tau_{\text{vis}}$, $t > \tau_{\text{diff}}$, viscosity and diffraction dissipate the UAP (decreasing η_0 while increasing z_0) and will finally become the leading terms of a quasilinear propagation equation.

V. SAMPLE TEMPERATURE CONTROL TO MEET THE KDV REQUIREMENTS FOR SOLITON OBSERVATION

At the highest laser fluences, where nonlinearity is expected to be the strongest, the heating of the sample may be an issue. Indeed, since the viscosity parameter increases drastically above 70 K, the KdV requirements may be nullified when the excitation power increases. To illustrate this issue, we will discuss the results of experiments where the acoustic pulse is generated in a 100-nm-thick chromium film which is slightly transparent. The UAP is detected in a chromium film as well after propagation through the GaAs(001) substrate which is then heated by the pump pulses. By varying the pump

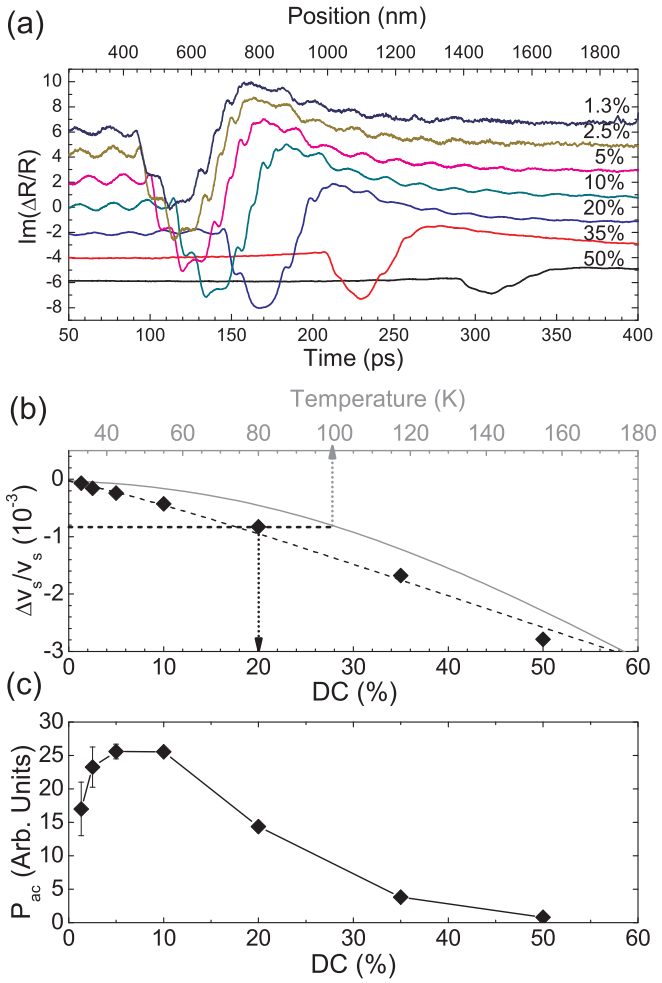

FIG. 3. Example of laser heating in ultrafast acoustic experiment in the case of a 100 nm chromium film as transducer on top of 370-μm-thick GaAs cooled down to $T_0 = 30$ K. The average power is changed while the energy per pulse is kept constant by controlling the duty cycle (DC). Average pump power is 1 W at DC = 100%. (a) UAPs measured for different DC with a vertical offset applied for the purpose of clarity. (b) Measurements (black diamonds) and calculated values (dashed line) for the relative change of velocity $\frac{\Delta v_s}{v_s}$(DC) (black scale). The corresponding temperature is provided by Ref. [22] and is given by $\frac{\Delta v_s}{v_s}(T)$ (gray curve, gray scale). (c) Acoustic power detected when varying the DC.

power while keeping the same energy per pulse (12.5 nJ) by adjusting the illumination time t_p, different acoustic pulses are detected. The results shown in Fig. 3(a) are obtained with the cryostat temperature set to 30 K and for different duty cycles DC $= \frac{t_p}{t_{\text{ref}}}$. A duty cycle of 100% corresponds to 1 W of laser pump power incident on the sample. When the mean power increases, the acoustic pulse is delayed, which is a clear signature of the stationary sample heating. Since the temperature dependence of the sound velocity is known, it is possible to estimate the temperature rise by extracting the change of velocity $\frac{\Delta v_s}{v_s}$(DC) from the experiments. The relative change of velocity $\frac{\Delta v_s}{v_s}$(DC) is obtained from the phase of the signal (after Fourier transform) which is averaged between 10 and 40 GHz to minimize the dispersion contribution. The results (black diamonds, black scale) are plotted in Fig. 3(b). The temperature dependence of the sound velocity is obtained from Ref. [22] where the temperature dependence at 56 GHz can be well fitted by $\frac{\Delta v_s}{v_s}(T) = A([1 + (\frac{T}{B})^C]^{1/C} - 1)$ with $A = -5.3(\pm 0.3)10^{-3}$, $B = 125(\pm 5)$ K, and $C = 2.9(\pm 0.1)$. The fitting curve is plotted in Fig. 3(b) (gray curve, gray scale). Once the heat capacity dependence with temperature [24] is taken into account, the measurements of $\frac{\Delta v_s}{v_s}(T)$ compare well with the expected values (dashed gray curve) plotted in Fig. 3(b). At DC = 50%, the stationary temperature reaches 170 K, 140 K above the set temperature. This spectacular effect under a high power (500 mW) is likely due to a poor thermalization of the sample, which can be modeled as a contact thermal resistance at the GaAs–cold finger interface. This result can be compared to those of a recent thermal study of pump-probe experiments on a GaAs substrate [25]. Using a different approach, a temperature rise of a few tens of Kelvins was estimated, and could indeed be well accounted for numerically with such a thermal resistance.

It is possible in fact to check experimentally that the attenuation may still be neglected within precisely controlled experimental conditions while generating high amplitude strain pulses. It is clear from Fig. 3(a) that the strain pulse amplitude decreases as the DC increases above 10% (i.e., $\frac{\Delta v_s}{v_s} < -4 \times 10^{-4}$). It is confirmed when the acoustic power P_{ac} carried by the UAPs is estimated after the propagation through the substrate [26]. Figure 3(c) displays the dependence on the DC of P_{ac}: above 10%, P_{ac} continuously drops to reach a value as low as $P_{\text{ac}}(50\%) \approx \frac{P_{\text{ac}}(10\%)}{32}$ [see Fig. 3(b)]. This is a clear signature of increasing acoustic attenuation with increasing DC. The decrease of P_{ac} observed at the lowest DC is not very significant (see error bars) since the finite time response of the AOM (around 8 ns) partially damps several pump pulses located at the front and the back of the gate which contains only $\approx$20 pulses at DC = 1.3%. Therefore the attenuation cannot be neglected any more when DC > 10%, i.e., when $\frac{\Delta v_s}{v_s} < -4 \times 10^{-4}$ or when the temperature goes above 80 K [see Fig. 3(b)]. Such temperature dependence of the attenuation of acoustic pulses has also been observed when the GaAs sample is efficiently cooled by a helium flow cryostat which was set to different temperatures above and below 80 K. Thanks to the good accuracy of the measurement of $\frac{\Delta v_s}{v_s}$ (of the order of 10^{-5}) it is possible to ensure experimentally by the right choice of DC that the sample temperature remains below 50 K, which allows one to safely ignore the viscosity effect as required for real KdV soliton observation. By checking that the sound velocity is independent of mean pump power at fixed energy/pulse, the DC has been set at 10% during the experiments performed on samples covered with Ti thin films, which are discussed below.

VI. OBSERVATION OF KdV SOLITONS

Figure 4 shows the UAP detected after propagation through a 370-μm-thick GaAs(001) substrate for different energies per pump pulse and different layer thicknesses of the transducer. As in Fig. 1, the signal curve displays a train of discrete transients traveling faster than the sound, which is typical of solitons. However, solitonic waves possess other more specific properties. In particular, the second property

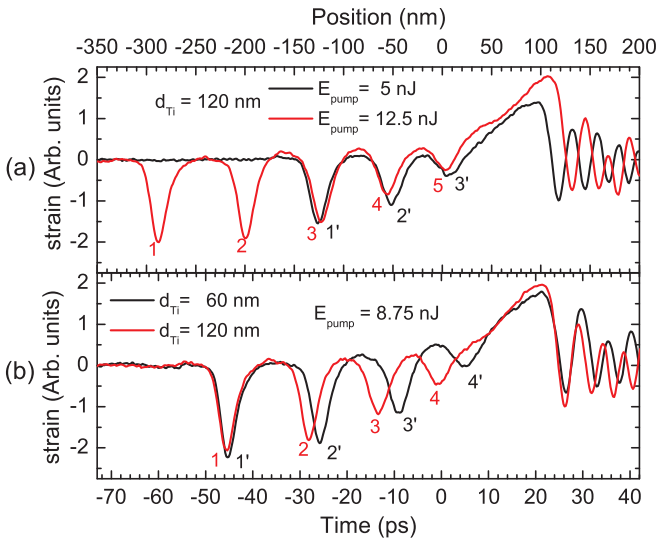

FIG. 4. Trains of solitons observed at 20 K (DC = 10%) for (a) different pump energies E_{pump} but same titanium film thickness $d_{\text{Ti}} =$ 120 nm and (b) different titanium film thicknesses d_{Ti} but same pump energy $E_{\text{pump}} = 8.75$ nJ.

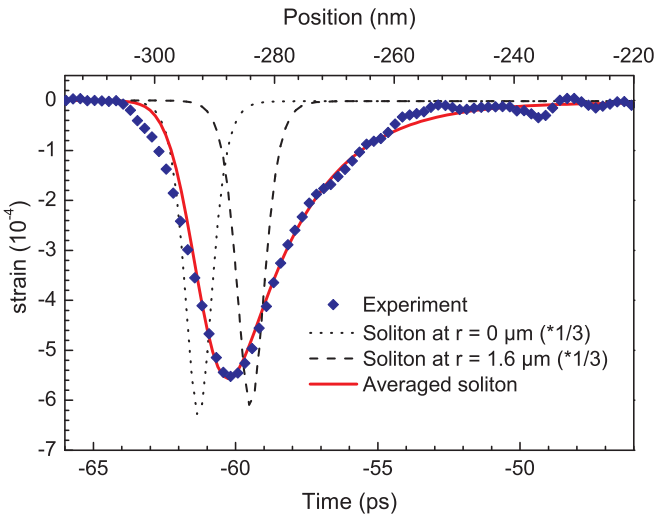

FIG. 5. Zoom on the fastest soliton profile for $d_{\text{Ti}} = 60$ nm and $E_p = 12.5$ nJ as measured by the interferometric setup. Expected soliton profile (solid line) when averaging over the probe spot. The soliton profile at $r = 0$ μm and $r = 1.6$ μm are plotted (dotted and dashed curves, respectively) scaled down by 3.

of a KdV soliton as recalled in the Introduction implies that different initial UAPs may lead to identical solitons if they share a common k value. Figures 4(a) and 4(b) display the strain pulses generated in Ti thin films 60 or 120 nm thick and detected in 60-nm-thick Ti film after propagation through the GaAs substrate. While Fig. 4(a) compares different energy/pulse E_{pump} but same film thickness $d_{\text{Ti}} = 120$ nm, Fig. 4(b) compares different film thicknesses d_{Ti} but same $E_{\text{pump}} = 8.75$ nJ. The initial strain pulse differs mainly by its amplitude in the former case [Fig. 4(a)], while it differs also by its width in the latter case [Fig. 4(b)]. The difference in the initial pulse shape is evidenced by differences in the train of solitons. Let us rank the solitons from the fastest to the slowest and use the quotation mark to distinguish solitons from different trains (i.e., different initial UAP). Solitons $1'$ and 3 in Fig. 4(a) and solitons 1 and $1'$ in Fig. 4(b) are almost identical. The same velocity means the same amplitude and the same width, as expected. Such observations are experimental evidence that the KdV soliton properties are entirely determined by a single parameter—its velocity, for example. In principle, it is possible, thanks to the time reversal property of the KdV equation, to numerically back-propagate the soliton distribution provided the soliton profiles follow the theoretical ones. Let us check whether this is the case.

Figure 5 offers a closer look at the shape of the fastest soliton detected at 12.5 nJ/pulse with $d_{\text{Ti}} = 60$ nm. The detected soliton shows an asymmetric shape in contrast to the KdV soliton which is symmetric, which implies the signal is not proportional to the strain amplitude. Indeed, the experiment is mostly sensitive to a superposition of solitons associated to different k parameters and/or different arrival times at the surface of the sample. To compute the detected soliton profile, one must consider an integral expression such as

$$\eta_{k_0}(z,t) = \iiint \eta_k(z,t) g(k,k',z_s)\, dk\, dk'\, dz_s \qquad (2)$$

where $g(k,k',z_s)$ weights the contribution of each soliton to the soliton shape of the k_0 parameter and can be expressed as a product of three different weight functions. Let us review the effects which are involved in the expression of $g(k,k',z_s) = g_{\delta k}(k,k') g_{\delta z_s}(z_s) g_{k_0}(k)$. The power fluctuations of the pump pulse do lead to a change δk of the k parameter and thus of the soliton detected from one pulse to the other. Since the laser noise is Gaussian, a typical weight function looks like $g_{\delta k}(k,k') = \frac{1}{\delta k\sqrt{2\pi}} e^{-(1/2)[(k'-k)/\delta k]^2}$. However, unlike previous experiments performed with amplified laser systems [6], it cannot be invoked as the main cause of soliton averaging. The pulse-to-pulse root mean square (rms) energy fluctuation over 10 min has been measured to be less than 0.5%, which means a fluctuation δk of less than 1.0%. The metallic film quality has also been asserted by measuring its rms roughness by atomic force microscopy. The KdV soliton profile is averaged over z_s to take into account the thickness fluctuation of the metallic film measured around $\delta z_s = 1.8$ nm (root-mean-square deviation). It can be compared to 0.6 nm for the bare GaAs substrate. This leads to the weight function $g_{\delta z_s}(z_s) = \frac{1}{\delta z_s\sqrt{2\pi}} e^{-(1/2)(z_s/\delta z_s)^2}$. Both of these effects induce a small increase of the soliton width as well as a small decrease of the soliton amplitude but the profile remains symmetric.

As previously suggested [2,6], the averaging of the surface displacement in the transverse direction by the probe spot affects the soliton shape as well. Indeed, the soliton properties have a radial dependence as illustrated in Fig. 5: solitons generated on the side (dashed curves) are slower than solitons generated at the epicenter (dotted curves). Such an effect can be computed by calculating the $k(\eta)$ values depending on the initial pulse strain η for a given pulse profile with the help of Eq. (1). The initial pulse profile is assumed to follow the pump profile such that $\eta(r) = \eta_0 e^{-(r/r_p)^2}$ with $r_p = 8$ μm. Once $k(\eta)$ is known, the soliton profile is averaged over r by taking into account the Gaussian probe profile

$\frac{1}{\pi r_s^2} e^{-(r/r_s)^2}$ with $r_s = 1.6$ μm. Overall, the spatial averaging can be written as an integral over the different k values from 0 to k_0 with $\eta(k_0) = \eta_0$ given the weight function $g_{k_0}(k) = \frac{1}{\eta_0}(\frac{r_p}{r_s})^2(\frac{\eta(k)}{\eta_0})^{(r_p/r_s)^2-1}\frac{d\eta}{dk}$. The soliton profile with nominal k_0 parameter is asymmetrically broadened since the profile is averaged over lower k value only (i.e., slower solitons). Note that a good approximation of $g_{k_0}(k)$ can be obtained for large strain amplitude soliton by assuming the k^2 values follow the strain profile (i.e., $k^2 = A\eta$).

The comparison between the experimental and the computed solitons for an initial UAP amplitude $\eta_0 = 1.37 \times 10^{-3}$ (fitting parameter) is shown in Fig. 5. The asymmetry of the detected soliton profile is well reproduced. For this experiment, it implies a soliton amplitude at $r = 0$ μm as large as $ak^2 = 1.9 \times 10^{-3}$ and a soliton width as short as $k^{-1} =$ 0.64 ps (i.e., 3.1 nm) (see dotted curved in Fig. 5). The spatial width appears to be comparable with the soliton widths measured in MgO [3] (2.7 nm for $ak^2 = 0.43 \times 10^{-3}$) and sapphire [6] (2.0 nm for $ak^2 = 3.4 \times 10^{-3}$) keeping in mind that the width of solitons scale like k^{-1}. Hence the computation confirms that the probe averaging effect can explain the measured soliton shape, while the other two effects, also introduced numerically, are much less significant. As a side note, a better fit can be obtained if a small photoelastic contribution is included after the averaging (not shown). Once the soliton amplitude is retrieved, the sensitivity of the setup can be calibrated (see the vertical scale of Fig. 5, which is not arbitrary).

While the probe spot is almost five times smaller than the pump spot (1.6 μm compared to 8.0 μm) the averaged soliton is still three times broader and smaller than the soliton expected at the epicenter. On the other hand, its arrival time is only delayed by 1 ps. The arrival time of the soliton at $r = 0$ μm can then be retrieved from the measurement with an accuracy better than 1%. Thanks to the unique properties of KdV solitons, it is then possible to get from the arrival time (i.e., the excess of sound velocity) the amplitude and the width of the soliton with good accuracy as well. Moreover, since the arrival time measurement allows one to retrieve the k parameters for each soliton, it seems possible to retrieve the initial UAP with the help of the inverse scattering method. Soliton distribution analyses like the one performed by Singhsomroje *et al.* [3] are then possible. (This is the topic of an upcoming report.)

VII. INITIAL PULSE RETRIEVAL

According to the two-temperature model of photothermal transduction in metallic thin films [27], the acoustic pulse profiles can be sorted into three categories:

(1) The exponentially decaying profile as given for weakly conducting metallic film and predicted by the one-temperature photothermal model.

(2) The square profile consistent with highly conducting metallic thin film, when the film thickness is smaller than the penetration depth of the photoexcited carriers [3].

(3) The Gaussian derivative profile which may be viewed as the intermediate case where the photocarrier penetration depth is not negligible but is smaller than the film thickness [6].

According to the inverse scattering method, an exponentially decaying profile should lead to a soliton distribution

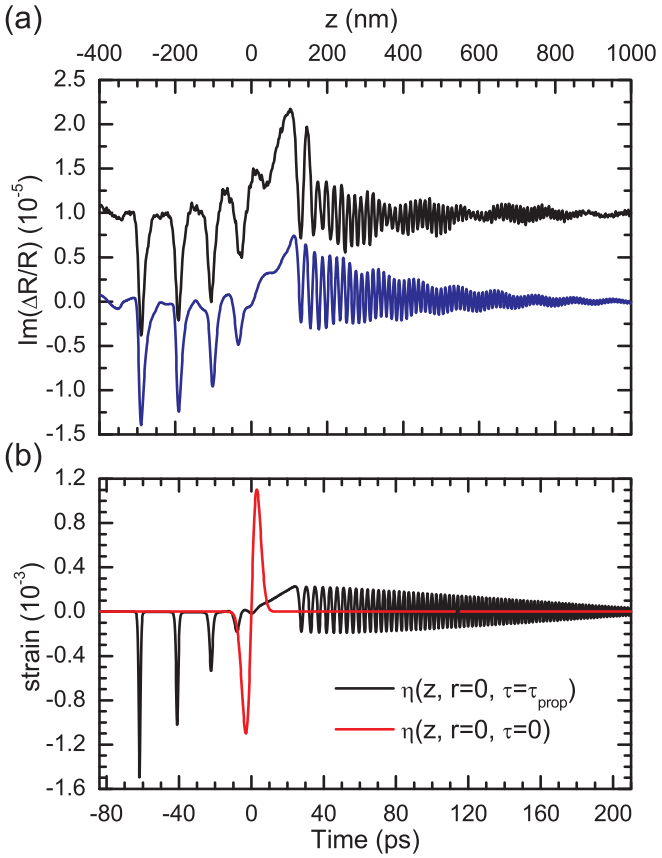

FIG. 6. (a) Ultrafast acoustics signal (black line) measured at 20 K (DC = 10%) for $E_{\text{pump}} = 12.5$ nJ and $d_{\text{Ti}} = 60$ nm and expected strain profile (blue line) computed with $\eta_0 = 1.083(\pm 0.006) \times 10^{-3}$ and $z_0 = 19.5$ nm. (b) Corresponding pulse profiles at $r = 0$ μm before propagation ($\tau = 0$ ns) and after propagation ($\tau = 77.4$ ns) through the substrate.

where the faster the solitons are, the further apart they are. In contrast, the square profile should lead to the opposite. Hence, it is straightforward to rule out these two initial profiles in the case of the thin Ti film. Indeed, measurements in the Ti film case show solitons which are more or less equidistant, which means the initial pulse must be quasiharmonic (Fig. 4). Since the Gaussian derivative profile measured at low laser fluence is close to a harmonic profile, it looks like a good candidate to fit the experiments. Indeed, Fig. 6(a) displays the measured and fitted signal using a Gaussian derivative profile as the initial pulse profile. The initial pulse width and the initial pulse amplitude are the only free parameters of the fit. The overall agreement strongly supports the use of the Gaussian derivative profile in Ti thin film cases. The resulting UAP is shown in Fig. 6(b) and the corresponding strain profile after propagation is drawn for $r = 0$ μm. It is interesting to note that the width parameter z_0 has to be 50% larger than the width measured at low pump power. It can be explained within the two-temperature model, which takes into account the heat diffusion by the electrons which is temperature dependent. A detailed study of this is out of the scope of this report but nicely illustrates how the study of acoustic soliton

distribution can help to investigate photothermal transduction mechnanisms up to the ablation threshold.

VIII. SUMMARY

The Korteweg–de Vries equation has been revisited in the framework of ultrafast acoustics in order to find the right experimental conditions to generate acoustic solitons. Emphasis is given on the laser heating of the sample which hampers the propagation of solitons. A way to deal with the thermal issue when performing nonlinear ultrafast acoustic experiments is demonstrated by carefully choosing a cryogenic working temperature and by imposing a low enough on/off time ratio for the pump beam. Then the existence of KdV-type solitons is demonstrated in a GaAs(001) substrate. Their intriguing properties have been illustrated experimentally and the very specific soliton profile is retrieved once the radial part of the signal is taken into account. Since the soliton amplitude is unambiguously determined by its velocity, its observation means a *de facto* calibration of the apparatus sensitivity. Moreover, the soliton properties as revealed by the inverse scattering method can be put to good use to study the photothermal strain generation by retrieving the initial pulse. Such measurements should be possible even at higher laser power where the photo-thermal strain generation becomes a highly nonlinear process. Practically, one can measure the soliton distribution created by the shock wave induced by the laser excitation in order to access fundamental material properties under strong light-matter interaction such as electronic conductivity, thermal conductivity, heat capacity, and so on. The accurate detection of KdV-type acoustic solitons opens new perspectives in ultrafast acoustics.

ACKNOWLEDGMENTS

The authors acknowledge financial support from MANGAS project (ANR 2010-BLANC-0424-02). They would like to thank Loïc Beccera and Silbé Majrab for their technical support and Jean Louis Thomas for very helpful discussions.

[1] M. J. Ablowitz and D. E. Baldwin, Phys. Rev. E **86**, 036305 (2012).
[2] H.-Y. Hao and H. J. Maris, Phys. Rev. B **64**, 064302 (2001).
[3] W. Singhsomroje and H. J. Maris, Phys. Rev. B **69**, 174303 (2004).
[4] B. C. Daly, T. B. Norris, J. Chen, and J. B. Khurgin, Phys. Rev. B **70**, 214307 (2004).
[5] E. Péronne and B. Perrin, Ultrasonics **44**, e1203 (2006).
[6] P. J. S. van Capel and J. I. Dijkhuis, Phys. Rev. B **81**, 144106 (2010).
[7] E. S. K. Young, A. V. Akimov, R. P. Campion, A. J. Kent, and V. Gusev, Phys. Rev. B **86**, 155207 (2012).
[8] R. M. Miura, SIAM Rev. **18**, 412 (1976).
[9] A. V. Scherbakov, P. J. S. van Capel, A. V. Akimov, J. I. Dijkhuis, D. R. Yakovlev, T. Berstermann, and M. Bayer, Phys. Rev. Lett. **99**, 057402 (2007).
[10] E. S. K. Young, A. V. Akimov, M. Henini, L. Eaves, and A. J. Kent, Phys. Rev. Lett. **108**, 226601 (2012).
[11] T. Berstermann, C. Bruggemann, A. V. Akimov, M. Bombeck, D. R. Yakovlev, N. A. Gippius, A. V. Scherbakov, I. Sagnes, J. Bloch, and M. Bayer, Phys. Rev. B **86**, 195306 (2012).
[12] A. Casiraghi, P. Walker, A. V. Akimov, K. W. Edmonds, A. W. Rushforth, E. De Ranieri, R. P. Campion, B. L. Gallagher, and A. J. Kent, Appl. Phys. Lett. **99**, 262503 (2011).
[13] M. Bombeck, A. S. Salasyuk, B. A. Glavin, A. V. Scherbakov, C. Bruggemann, D. R. Yakovlev, V. F. Sapega, X. Liu, J. K. Furdyna, A. V. Akimov, and M. Bayer, Phys. Rev. B **85**, 195324 (2012).
[14] M. Bombeck, J. V. Jager, A. V. Scherbakov, T. Linnik, D. R. Yakovlev, X. Liu, J. K. Furdyna, A. V. Akimov, and M. Bayer, Phys. Rev. B **87**, 060302 (2013).
[15] N. C. R. Holme, B. C. Daly, M. T. Myaing, and T. B. Norris, Appl. Phys. Lett. **83**, 392 (2003).
[16] B. C. Daly, N. C. R. Holme, T. Buma, C. Branciard, T. B. Norris, D. M. Tennant, J. A. Taylor, J. E. Bower, and S. Pau, Appl. Phys. Lett. **84**, 5180 (2004).
[17] H. J. Maris and S. Tamura, Phys. Rev. B **84**, 024301 (2011).
[18] T. Kawasaki, S. Tamura, and H. J. Maris, J. Phys.: Conf. Series **92**, 012091 (2007).
[19] P. J. S. van Capel, E. Péronne, and J. I. Dijkhuis, Ultrasonics **56**, 36 (2015).
[20] D. P. DiVincenzo, Phys. Rev. B **34**, 5450 (1986).
[21] R. Legrand, A. Huynh, B. Jusserand, B. Perrin, and A. Lemaitre, Phys. Rev. B **93**, 184304 (2016).
[22] W. Chen, H. J. Maris, Z. R. Wasilewski, and S. I. Tamura, Philos. Mag. B **70**, 687 (1994).
[23] B. P. Newberry and R. B. Thompson, J. Acoust. Soc. Am. **85**, 2290 (1989).
[24] J. S. Blakemore, J. Appl. Phys. **53**, R123 (1982).
[25] S. Shihab, L. Thevenard, A. Lemaitre, J. Y. Duquesne, and C. Gourdon, J. Appl. Phys. **119**, 153904 (2016).
[26] E. Péronne, E. Charron, S. Vincent, S. Sauvage, A. Lemaitre, B. Perrin, and B. Jusserand, Appl. Phys. Lett. **102**, 043107 (2013).
[27] T. Saito, O. Matsuda, and O. B. Wright, Phys. Rev. B **67**, 205421 (2003).